JOURNAL OF APPLIED ELECTROCHEMISTRY 23 (1993) 996–1010

Ozone generation via the electrolysis of fluoboric acid using glassy carbon anodes and air depolarized cathodes

P. C. FOLLER*,

OxyTech, Inc., 141B Albright Way, Los Gatos, CA 95030, USA

G. H. KELSALL

Imperial College, Department of Mineral Resources Engineering, Prince Consort Road, London SW7 2BP, UK

Received 24 November 1992; revised 27 January 1993

An electrochemical ozone generation process was studied wherein glassy carbon anodes and air depolarized cathodes were used to produce ozone at concentrations much higher than those obtainable by conventional oxygen-fed corona discharge generators. A mathematical model of the build up of ozone concentration with time is presented and compared to experimental data. Products based on this technology show promise of decreased initial costs compared with corona discharge ozone generation; however, energy consumption per kg ozone is greater. Recent developments in the literature are reviewed.

Nomenclature

A	electrode area (m^2)
Ar^*	modified Archimedes number, $d_b^3 g\alpha_G/v^2(1-\alpha_G)$
$C_{O_3(aq)}$	concentration of dissolved ozone ($mol\,m^{-3}$)
C_{O_3i}	concentration at interface ($mol\,m^{-3}$)
C_{O_3l}	concentration in bulk liquid ($mol\,m^{-3}$)
D	diffusion coefficient ($m^2\,s^{-1}$)
E	electrode potential against reference (V)
F	charge of one mole of electrons ($96\,485\,C\,mol^{-1}$)
g	gravitational acceleration ($9.806\,65\,m\,s^{-2}$)
i	current density ($A\,m^{-2}$)
i_l	limiting current density ($A\,m^{-2}$)
I	current (A)
j	material flux per unit area ($mol\,m^{-2}\,s^{-1}$)
k_{obs}	observed rate constant ($mol^{-1}\,s^{-1}$)
k_t	thermal conductivity ($J\,s^{-1}\,K^{-1}$)
L	reactor/anode height (m)
N_{O_3}	average rate of mass transfer ($mol\,m^{-2}\,s^{-1}$)
Q	heat flux ($J\,s^{-1}$)
r_i	radius of anode interior (m)
r_a	radius of anode exterior (m)
r_c	radius of cathode (m)
R	gas constant ($8.314\,J\,K^{-1}\,mol^{-1}$)
Sc	Schmidt number, ν/D
Sh	Sherwood number, $k_m d_b/D = i_L d_b/zFD[O_3]$
t	time (s)
T_i	temperature of inner surface (K)
T_o	temperature of outer surface (K)
U	reactor terminal voltage (V)
v	electrolyte linear velocity ($m\,s^{-1}$)
V	volume (m^3)
V_{O_3}	volume of ozone evolved ($10^{-6}\,m^3\,h^{-1}$)
z_i	number of Faradays per mole of reactant in the electrochemical reaction

Greek symbols

α_G	gas phase fraction in the electrolyte
δ	(mean) Nernst diffusion layer thickness (m)
Φ	fractional current efficiency
η	overpotential (V)
ν	electrolyte kinematic viscosity ($m^2\,s^{-1}$)
ρ	electrolyte resistivity ($V\,A^{-1}\,m$)

1. Introduction

1.1. *Limitations of corona discharge and ultra-violet excitation*

Development of electrochemical ozone generation methods is of interest because of three clear problems with the conventional corona discharge and ultra-violet excitation ozone generation methods: high operating costs, high capital costs, and low ozone concentrations.

The low ozone concentrations obtained from conventional generation methods limit the effectiveness of ozone as a viable oxidant in many potential applications. Without mechanical refrigeration, the maximum concentrations that may be generated by air fed and oxygen fed corona discharge are approximately 2.5 and 7.5 wt %, respectively. These concentrations can be achieved only far from the energetic minima and with a significant derating of the output capacity of the generation equipment used. Ultraviolet excitation

* Current address E-TEK, Inc., 1 Mountain Road, Framingham Industrial Park, Framingham, MA 01701, USA

0021-891X

generates ozone in the range of several thousand parts per million.

Electrochemical approaches can generate far higher ozone concentrations than available conventionally. Advantages can be expected in mass transfer, reaction kinetics, contactor and gas handling equipment sizing, product through-put, and perhaps decreased losses through ozone decomposition during handling. (Through ozone is generally cited to have a half-life in air of 20 to 30 min, this range is only a practical guideline. The actual rate constants for the homogeneous gas-phase decomposition show that far longer half-lives are indeed achieved if the effects of vessel walls and materials of construction can be decreased.)

Strictly comparing the operating costs of the electrochemical and corona generation methods on a $kWh\,kg^{-1}$ basis, it is not possible to project an advantage for an electrochemical approach. The generation of ozone by the anodic oxidation of water is more endothermic than generation via dissociation and recombination of oxygen. Further, both oxygen reduction and ozone evolution require large overpotentials for electrochemical reactions. Parity with the generation of 1 to 2 wt % ozone via air fed corona discharge is too optimistic a development goal. Thus, for an electrochemical approach to have economic advantages, capital cost and improvements in contacting will always have to be weighed against a specific electrical energy consumption penalty versus air and oxygen fed corona discharge.

Disregarding the limitations of generation methods, ozone should be a very useful industrial chemical. It is attractive for its high oxidation potential and lack of residuals which can cause difficulties in the application of chlorine-based oxidants. Its uses range from those requiring small, $0.005\,kg\,day^{-1}$, generators all the way to 50 to $5\,000\,kg\,day^{-1}$ systems such as used in many cities for potable water treatment. Many 'niche' market opportunities exist in speciality water treatment, surface sterilization, bleaching, materials processing, waste treatment, and the like. Certain of these, such as the treatment of cooling water, would find very high concentrations advantageous, and are more sensitive to capital cost rather than specific electrical energy consumption.

1.2. *Electrochemical methods*

Ozone has been generated electrochemically in three ways thought to be commerically relevant (through other approaches will be discussed).

Ozone may be evolved directly into a stream of relatively pure water from the back side of a porous (lead dioxide) anode in contact with a solid polymer perfluorinated sulphonic acid membrane electrolyte [1–3]. This method was first developed by Asea Brown Boveri (ABB) of Switzerland and was trademarked as the Membrel® process. This method has the advantage of dissolving a high concentration of ozone into water, and thus, to some extent, eliminates problems of contacting gas-phase ozone into water. The ozone-containing pure water stream may be admixed into a larger volume of impure water. Very high current densities (greater than $10\,kA\,m^{-2}$) are possible; however, the low (15%) current efficiency leads to a high specific electrical energy consumption with hydrogen evolution as the cathodic process. Water balance and thermal management present no special problems in this method. Permelec Electrode (Japan), Chlorine Engineers (Japan), Sasakura (Japan), and l'Air Liquide (France) under licence from ABB (Switzerland) offer products based on this approach [4, 5].

The Membrel® cell approach to electrolytic ozone generation has recently been extended to incorporate the use of oxygen cathodes by Permelec Electrode Corporation (Japan). Figure 1 shows the current efficiency and cell voltage of a laboratory cell operated over a period of three months [6]. Although the specific electrical energy requirement was decreased compared with those when hydrogen evolution was the cathodic process, the principal incentive for oxygen cathode use is the elimination of hydrogen handling. The fuel cell cathode material used is of a type which can be supplied by E-TEK, Inc. [7].

Ozone may also be evolved from a system optimized for current efficiency using a more specialized electrolyte, fluoboric acid, for instance [8–12]. In this approach ozone is also formed by the six electron

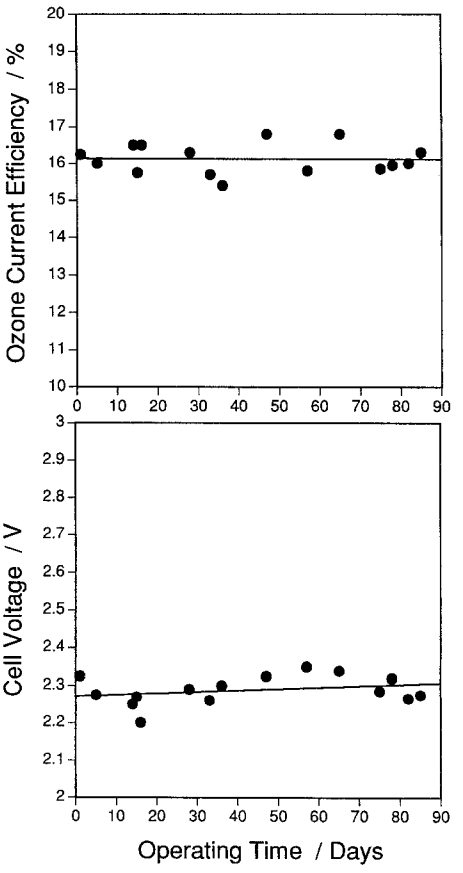

Fig. 1. Cell voltage and current efficiency for Permelec Electrode Ltd solid polymer electrolyte ozone generator [6].

decomposition of water, which, in this variant of the technology, is supplied by the operation of an air cathode. The use of an air cathode eliminates hydrogen management problems, lowers cell voltage, and decreases thermal management requirements. It is this latter approach that the balance of this paper discusses.

2. Process chemistry

2.1. *Electrochemical reactions*

The process chemistry involves decomposition of water to form a mixture of ozone and oxygen at the anode; this water is then replaced by the reduction of atmospheric oxygen at the cathode. Figure 2(a) and (b) depicts the electrochemical reactor designs used. Figure 3 presents the flow sheet for an ozone generator based on the reactors of Fig. 2. The following reaction decribe the ozone generation process, being ozone current efficiency:

Desired anode reaction:

$$\Phi(3H_2O = O_3 + 6H^+ + 6e^-) \quad (1)$$

$$E/V = 1.511 - 0.0591\,\mathrm{pH} + 0.0099 \log P_{O_3}$$

Anode side reaction:

$$(1 - \Phi)(2H_2O = O_2 + 4H^+ + 4e^-) \quad (2)$$

$$E/V = 1.229 - 0.0591\,\mathrm{pH} + 0.0148 \log P_{O_2}$$

Overall anode reaction:

$$(\Phi + 2)H_2O = \Phi O_3 + (1 - \Phi)O_2 + (2\Phi + 4)H^+ + (2\Phi + 4)e^- \quad (3)$$

Cathode reaction:

$$(2\Phi + 4)/4O_2 + (2\Phi + 4)H^+ + (2\Phi + 4)e^- = (2\Phi + 4)/2H_2O \quad (4)$$

Net process:

$$(\Phi + 2)/2O_2 = \Phi O_3 + (1 - \Phi)O_2 \quad (5)$$

The specific electrical energy consumption (*SEEC*) for the process is given by:

$$SEEC/\mathrm{kWh\,(mol\,O_3)^{-1}} = 0.1608\,U\,\Phi^{-1} \quad (6)$$

where U is the cell voltage. The current efficiency (Φ) for ozone generation is numerically equivalent to the volume per cent efficiency that is anodically evolved.

The current efficiencies cited below are calculated from data obtained from a Griffin Technics (Lodi, New Jersey) model 1003-HC ultraviolet spectrophotometric ozone monitor. The calculations made were based on the following relationship:

$$\Phi/\% = 200(V_{O_3})/(456.3\,A - V_{O_3})$$

where V_{O_3} = (vol% measured) × (flow rate) in $10^{-6}\,m^3\,h^{-1}$ and vol% (in air) = 2900/4800/(wt% − 19).

It should be noted that the feed air may be filtered ambient air. As the electrolyte used is an acid, CO_2 absorption by the electrolyte is not the problem it would be with alkaline electrolytes. If organics or other contaminants are captured by the electrolyte, the high concentrations of dissolved ozone have proved capable of oxidizing them totally; thus, no special precautions with feed air are required.

In electrochemical ozone generation, it is not possible to produce NO_x contaminants (as in the case of air-fed corona discharge when feed air is not dried to the recommended −50 to −60 °C dew point).

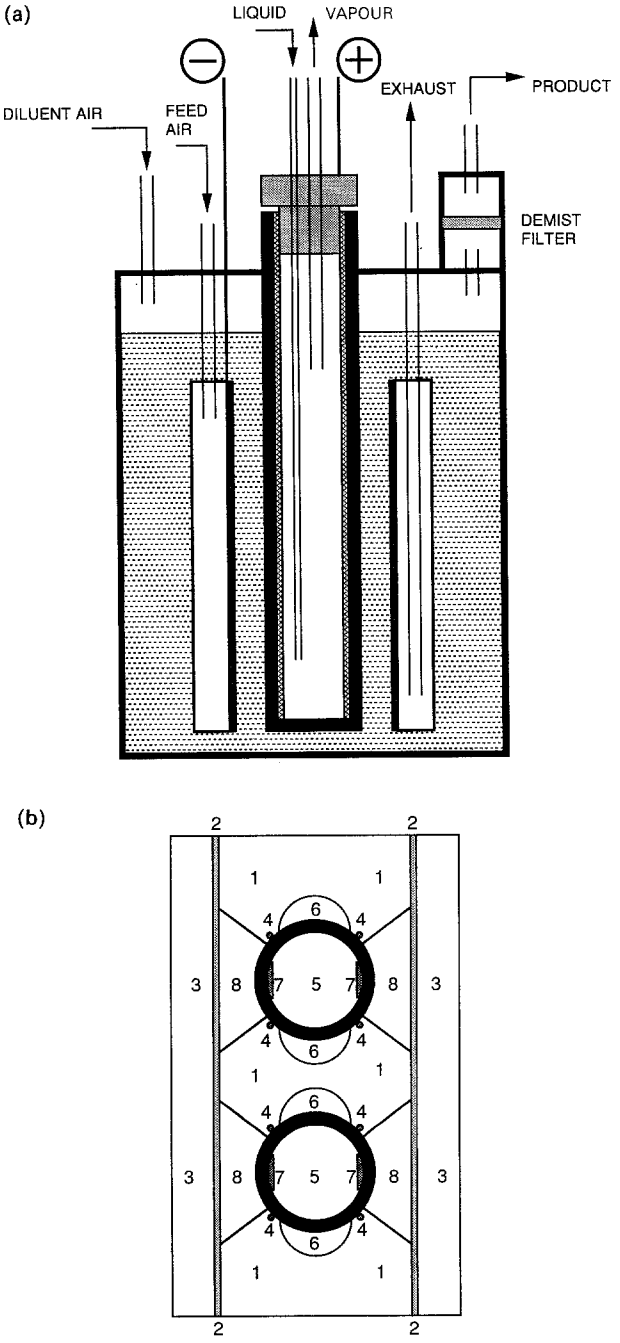

Fig. 2. Reactor designs: (a) concentric cylinder reactor; (b) planar cathode/tubular anode reactor [24] showing: (1) plastic mounting block, (2) air cathode, (3) air feed plenum, (4) anode seal, (5) refrigerant expansion/circulation pathway, (6) electrolyte downward circulation pathway, (7) metallic current contacts to glassy carbon anode, and (8) actual electrolyte.

2.2. *Electrolyte*

Fluoboric acid was chosen for a combination of properties that make it uniquely well-suited for electrochemical ozone evolution. It is non-oxidizing and nondehydrating; however, it is highly corrosive,

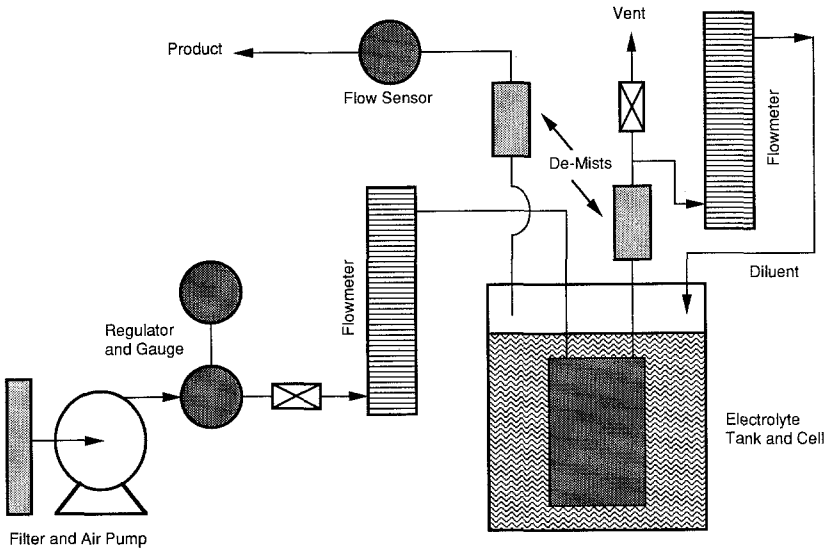

Fig. 3. Schematic of ozone generator.

and the toxicity may be grouped with the inorganic fluorides. It is neither electrochemically oxidized nor reduced under the range of reactor operational conditions, though the following reactions are predicted thermodynamically to be possible:

$$H_2BO_3H_3BO_32H_2O_2^- + 8HF + 3H^+ + 4e^- \Leftrightarrow 2BF_4^- + 10H_2O \quad (7)$$

$$E/V = 2.4701 - 0.0444\,pH - 0.0148\log(BF_4^-) + 0.0148\log(H_2BO_3H_3BO_32H_2O_2^-)$$

$$H_2BO_3H_3BO_32H_2O_2^- + 4F_2O + 19H^+ + 20e^- \Leftrightarrow 2BF_4^- + 14H_2O \quad (8)$$

$$E/V = 2.132 - 0.0562\,pH - 0.0059\log(BF_4^-) + 0.0030\log(H_2BO_3H_3BO_32H_2O_2^-)$$

$$H_2BO_3H_3BO_32H_2O_2^- + 4F_2 + 11H^+ + 12e^- \Leftrightarrow 2BF_4^- + 10H_2O \quad (9)$$

$$E/V = 2.7499 - 0.0542\,pH - 0.0099\log(BF_4^-) + 0.0049\log(H_2BO_3H_3BO_32H_2O_2^-)$$

No anodic perborate formation, nor F_2 or F_2O evolution have been observed. However, fluoborate ions are subject to hydrolysis by reactions such as

$$BF_4^- + H_2O \Leftrightarrow BF_3OH^- + HF \quad (10)$$

$$\log\{(BF_3OH^-)/(BF_4^-)\} = -2.23 - \log(HF)$$

$$BF_4^- + 2H_2O \Leftrightarrow BF_2(OH)_2^- + 2HF \quad (11)$$

$$\log\{(BF_2(OH)_2^-)/(BF_4^-)\} = -4.67 - 2\log(HF)$$

$$H_3BO_3 + 4HF \Leftrightarrow BF_4^- + 3H_2O + H^+ \quad (12)$$

$$\log\{(BF_4^-)/(H_3BO_3)\} = 7.41 + pH + 4\log(HF)$$

Such formation of HF and BF_3OH^- ions is especially prevalent at lower concentrations [13, 14] but may be suppressed by addition of approximately 3 wt % boric acid, which manufacturers add to their 48 wt % product to control HF vapour pressure. Low (p.p.m.) levels of HF appear in the cathode exhaust and product gases. To date this has not been judged a problem for the intended uses of the technology. (The thermodynamic relationships presented here were calculated from critically assessed data [15]; parentheses refer to activities rather than concentrations.)

Fluoboric acid at 48 wt % remains liquid to −78 °C, and thus the material is an ideal candidate for processes employing refrigeration. Fluoboric acid exists only as dissolved ions (H_3O^+ and BF_4^-) and thus it has no undissociated state vapour pressure. Also, being entirely dissociated, fluoboric acid is highly conductive, though Fig. 4 shows a penalty in conductivity at the higher fluoboric acid concentrations of interest in ozone generation.

The product stream must be demisted of fluoboric acid droplets. This can be accomplished with a column of (hydrophilic) PVC pellets, followed by the use of Teflon® microfilters. This technique was found not to decompose and the materials proved stable to the acid/ozone environment.

Fluoboric acid at 60 wt % (6.8 kmol $HBF_4\,m^{-3}$) concentration was prepared by vacuum evaporation of commerical 48 to 50 wt % compositions at −100 kPa and 45 °C. A 0.2 m diameter 1.5 m long tubular boiler heated with an internal coil circulating hot water produced 2 $dm^3\,h^{-1}$. Density measurements confirmed the resultant concentrations.

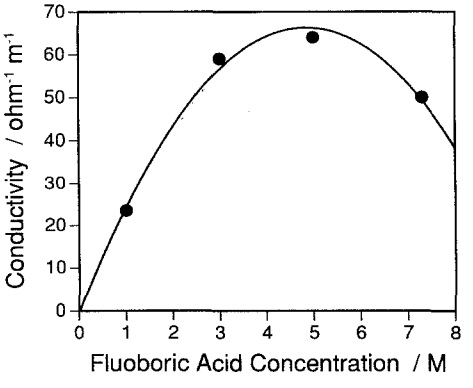

Fig. 4. Conductivity of fluoboric acid at 17 °C.

2.3. *Anodes*

Glassy carbon was selected as the anode material, from the very limited range of materials suitable for ozone evolution. The electrochemical ozone generation behaviour of platinum, α and β-lead dioxide, certain DSA coatings, and glassy carbon has been reported in the literature. Platinum is too costly for practical application and produces high current efficiencies only at very low temperature [16, 17]. Lead dioxide is capable of relatively high current efficiencies [18]. However, it suffers from severe stability problems [19] unless it is operated in neutral buffered electrolytes which are incapable of high current efficiencies [20, 21], or is pressed against an anion exchange membrane so that active material is not lost continuously [1–3]. DSA-type materials have not proved stable in ozone evolution, and have shown very poor current efficiencies [23].

Glassy carbon is not as stable as it is in high concentration fluoboric acid in any other electrolytes investigated. In fluoboric acid, the rate of attack decreases after an initial period (probably due to gradual electrochemical fluorination of surface functionality). Anode wear results from CO_2 production, perhaps arising from decarboxylation of surface carboxylic acid structures. It is also possible that erosion progresses via CF_4 or other fluorocarbon gases, formed by reactions such as

$$CF_4(g) + H_3BO_3 + 3H^+ + 4e^- \Leftrightarrow C + BF_4^- + 3H_2O \quad (13)$$

$$E/\mathrm{V} = 1.5406 - 0.0444\,\mathrm{pH} - 0.0148\log(BF_4^-) - 0.0148\log(H_3BO_3)$$

No production of coloured humic and/or fulvic acid materials was observed. Though there is a potential for formation of certain low molecular weight carboxylic acids, no characteristic odours have been detected even after prolonged electrolysis.

High current efficiencies are possible with glassy carbon anodes. Unlike in other electrolytes (e.g. sulphuric acid), glassy carbon anodes are sufficiently inert to merit detailed evaluation and optimization of experimental variables. It was found that anode erosion is a function of temperature, current density, and water activity. It may be minimized by using high concentrations of fluoboric acid at the lowest possible temperatures and current densities consistent with economic goals.

Higher concentrations of fluoboric acid not only decreased anode corrosion, but enhanced ozone yield. The best results, from both points of view, were obtained in specially prepared 60 wt % fluoboric acid (commercial grade is 48 to 50 wt %). Figure 5 shows the upward trend of anode current efficiency with increased fluoboric acid concentration; these data were taken using a small anode in a large volume of electrolyte. Figure 6 indicates the effect of extending the concentration range in Fig. 4 to specially

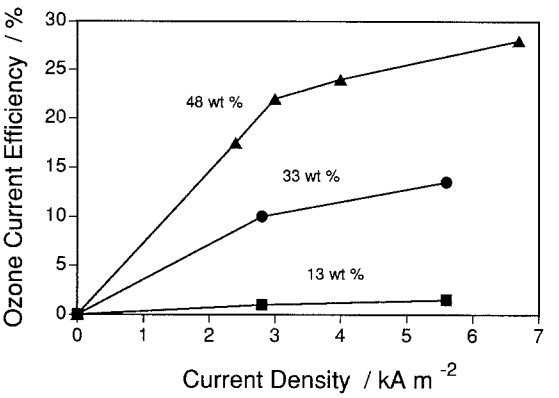

Fig. 5. Effect of fluoboric acid concentration on current efficiency. Results from $3.0 \times 10^{-4}\,m^2$ cell. Highest concentration (48–50 wt %) commercially available fluoboric acid was used.

prepared 62 wt % fluoboric acid, though the later data were taken in a planar cathode/tubular anode reactor discussed in Section 3.1. [24].

The rate of anode wear was a strong function of fluoboric acid concentration, current density, and temperature; however, under conditions of 60 wt % HBF_4 concentration, $3\,kA\,m^{-2}$, and using the expansion of refrigerant R502 to create an anode interior temperature of −15 to −20 °C, the rate of carbon loss corresponded to a wear rate of $1.5\,mm\,year^{-1}$, as measured via micrometer measurements over the course of 40 days of electrolysis. However, a much more rapid initial loss was observed within the first hour of operation, during which a stable surface was formed and some particulate carbon was lost from the anode.

The use of higher fluoboric acid concentrations to achieve increased current efficiencies for ozone generation is limited by intermittent anode passivation at high current densities. For example, in 60 wt % electrolyte, the stoichiometry of which is $H_3O^+BF_4^-$, Fig. 7 indicates that this occurred after an induction time of about 25 min under the particular conditions used. Apparent anode potentials as high as 15 Vvs SHE were observed, due to the so called 'anode effect', as observed, for example, in the electrolysis of molten fluorides using carbon anodes [25]. Use of lower temperatures appeared to encourage the formation

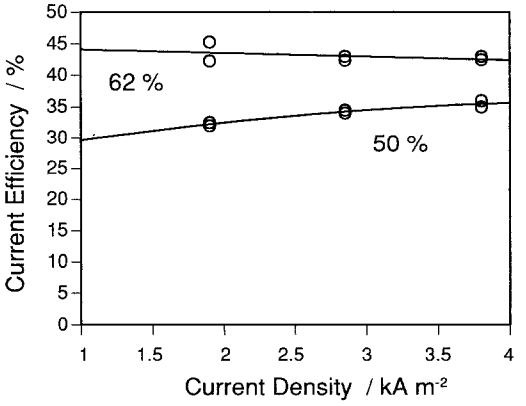

Fig. 6. Effect of fluoboric acid concentration on current efficiency. Results from planar/tubular reactor. Temperature: −5 °C. Fluoboric acid of 62 wt % concentration specially prepared [24].

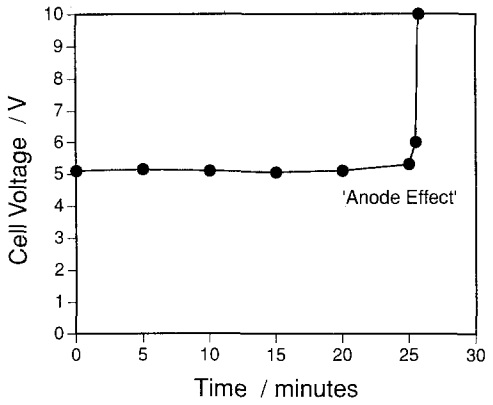

Fig. 7. 'Anode effect' in 60 wt % fluoboric acid. Current density of 4 kA m^{-2}. Concentric cylinder reactor. Glassy carbon prepared at 1000 °C. Temperature: −5 to −10 °C.

of the passive layer, which was transient, in that passivity was removed by a period at open circuit. The passivation probably resulted from the surface coverage of fluorinated carbon increasing with increasing current density. Its high hydrophobicity would cause oxygen, ozone and possibly fluorinated carbon gases to tend to adhere, depending on the prevailing hydrodynamic shear forces, which were found to diminish the susceptibility of the anode to passivation. Under the required operating conditions, oxygen adsorption would be dominant, resulting in a hydrophilic surface; hence, stable and reliable operation appeared to be achievable at a fluoboric concentration of 60 wt % in 'open' cell designs with judicious electrolyte circulation and gas removal provisions.

Different properties of glassy carbon result when different starting resin and different heat treatment temperatures are used in the formation of the glassy carbon. These typically range between 1000 and 3000 °C. Different heat treatment temperatures produce materials than exhibit different stabilities and ozone current efficiencies. At higher heat treatment temperatures, the resultant glassy carbon is more sp^2 (rather than sp^3) in character, and offers less corrosion resistance than reported above. However, higher heat treatment carbons also appear to show less susceptibility to the 'anode effect'. The thermal conductivity of material produced at 3000 °C heat treatment temperatures (8.0 J m^{-1} s^{-1} K^{-1}) is higher by a factor of two than material produced at 1000 °C. This is useful in producing lower anode surface temperatures. Gas evolution patterns on 1000 °C and 2500 °C material are also markedly different: large adherent bubbles on the former, and small, continuously released bubbles on the latter. The fraction of sp^2 to sp^3 surface functionality may affect the extent to which the surface fluorinates, and the resultant hydrophobic properties.

2.4. *Air cathodes*

Air cathodes using dispersed platinum on carbon/fluorocarbon sinters exhibited very poor oxygen reduction kinetics and unusual wetting properties in

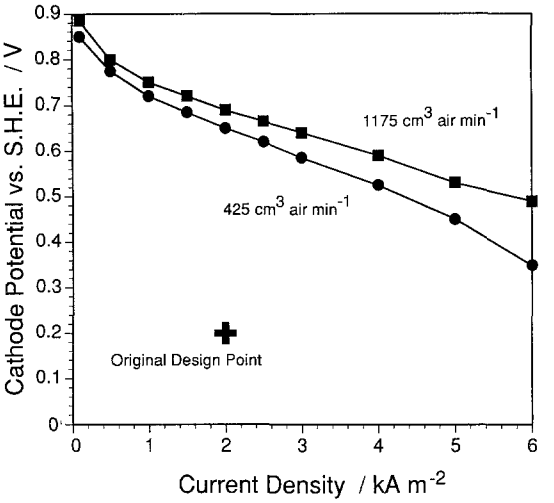

Fig. 8. Air cathode polarization behaviour in 48 wt % fluoboric acid at 25 °C.

fluoboric acid against experience in more conventional electrolytes. It was determined that the use of platinum black in the reaction layer of the air electrodes was, over the near term, necessary to achieve sufficient reaction rates. This was also partially due to the low electrolyte temperatures required, which varied at steady state from 0 to 20 °C, depending on the current passed in the 0 to 40 A, 2.7 dm^3 cells. Figure 8 shows the polarization of a Pt-black containing cathode, the composition of the reaction layer in this case being 5 wt % Teflon® with a 150 g m^{-2} loading of Pt-black. The data in Fig. 9, for an early poorly performing cathode, show that all else being equal, air electrodes apparently exhibit better performance in low concentrations of fluoboric acid.

It is anticipated that the lifetimes of the air electrodes in this application should prove fairly long, as they operate at low temperature. Figure 10 shows the time dependence of cathode polarization over 30 days, though over 210 days of operation have been achieved in a voluntarily terminated trial. Failure mechanisms appear to be gas feed layer wetting over

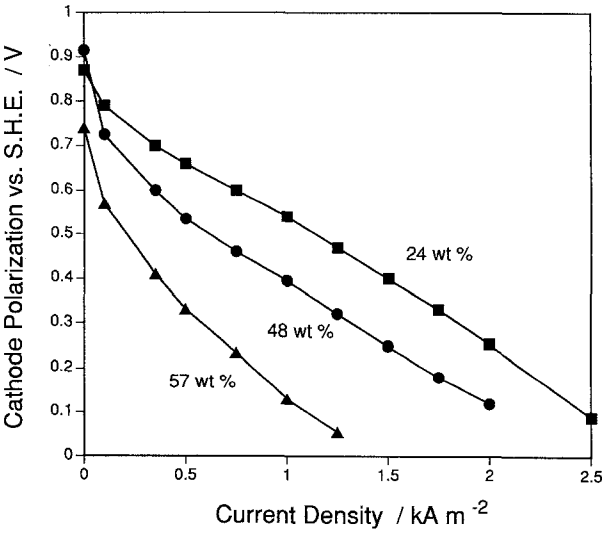

Fig. 9. Performance of air cathode as a function of fluoboric acid concentration.

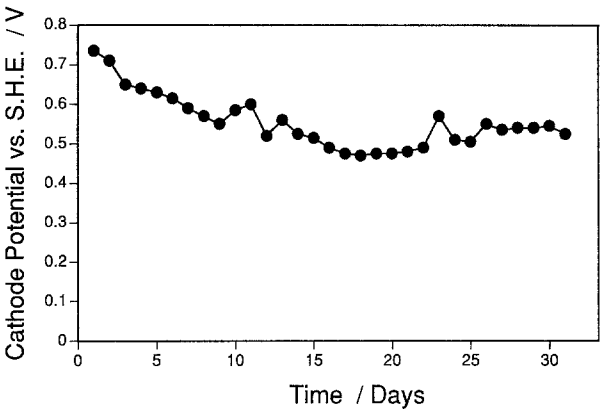

Fig. 10. Long-term air cathode performance at 30 to 35 °C.

the long term and possibly, in the shorter term, the poisoning of the platinum catalyst potentially caused by adsorption of organic material resulting from the (slow) anode corrosion. This hypothesis is based on the observation of cathode performance being restored subsequent to brief current reversals at very low current density and following washing with acetone, which turned yellow, indicating removal of organic material from the cathode. The simulation reactors, in which this testing was performed allowed an anode temperature of 40 °C, at which corrosion was enhanced severely over that observed at the targeted −10 °C surface temperatures. It was found that open circuit periods (initially studied over a cycle of 5 min off for every 65 min on) substantially increased electrode life [26]. Oxidation of adsorbed organics, or reduction of internal water content via diffusion are possible explanations.

The cathodes were formed on expanded silver which was gold plated in order to prevent attack of the silver, should it have come into contact with electrolyte containing dissolved ozone. (Fluoboric acid alone does not affect silver; however, with dissolved ozone present, serious corrosion can occur leading to the accumulation of insoluble light brown solids. The expanded metal substrate was placed in an extremely hydrophobic gas feed layer (behind layers of high surface area carbon and platinum black which catalyse the decomposition of ozone) so that it remained dry and protected. Thus, the gold plating prevented an intergranular corrosion of unprotected silver that otherwise would have resulted in a powdery current collector and associated loss of strength.

Water was both formed in the cathodes and was drawn into them by the electromigration of hydrogen ions. Thus, the concentration of fluoboric acid within the cathode was lower than in the bulk of the electrolyte. There was a higher water vapour pressure behind the cathodes than over the surface of the electrolyte, due to Laplace pressure effects resulting from the small radius of curvature of the hydrophobic pores in the PTFE-bonded cathodes. However, the concentration developed within the pores of the cathode is still hygroscopic, so that water is absorbed into the electrolyte at the cathodes.

Introducing diluent through the electrolyte rather than over it, or after the cell itself, the rate of water gain was measured with a Protimeter (Marlow, Bucks., UK) humidity sensor over a 10 day period (at 40 A operation) when ambient humidity averaged 50 to 70%. The water gain amounted to 0.25 dm^3 out of a total electrolyte volume of 2.7 dm^3 at 4 wt % ozone concentration.

Ozone was not found in the cathode exhaust stream either during the operation of the cells or after shutdown of current. Under operation, the catalytic action of the high surface area carbon and platinum combined with the passage of cathodic current, served to decompose ozone before it diffused from the electrolyte into the feed air chamber, due to ozone's instability with respect to oxygen:

$$O_3(g) \Leftrightarrow 1.5O_2(g) \qquad (14)$$

$$\log pO_3 = -28.59 + 1.5 \log pO_2$$

At shutdown, the catalytic effects alone were adequate to prevent crossover of dissolved ozone.

The cathodes are activated using a 20 min soak period, followed by a 10 A m^{-2} of anodic current to induce wetting, followed by gradual increases in cathodic current density over approximately 2 h.

3. Device design

3.1. *Small-scale (40 A) reactors*

The reactor design originally chosen for the initial small-scale demonstration of the technology was based on concentric cylinders: a tubular anode and a surrounding air cathode, as shown in Fig. 2(a). The design offered a differential of approximately 2 : 1 in cathode to anode area. Thus, as it was expected that high rate room-temperature air cathodes would prove difficult to develop, cathode current density need reach only one half the 4 kA m^{-2} anode current density, at which ozone current efficiency approached a plateau value in large volumes of cooled electrolyte. Further, as the anode surface must be cooled in order to achieve high current efficiency, the cylindrical geometry had an advantage in that the anode may be readily cooled while allowing the cathode to operate at higher temperatures, which are favourable to electrochemical performance.

The cathodes were solvent-cemented to a PVC cage that surrounded the anode. A specially prepared solvent cement using dissolved long-chain PVC polymer in tetrahydrofuran was used.

The resultant 40 A cell cassette was designed with a 0.010 to 0.0140 m^2 active anode area using a 0.0254 m o.d. glassy carbon tube with a 0.010 m interelectrode gap. The cassette was designed to be submerged in electrolyte, which was circulated through a bottom entrance and a top exit via bubble lift. Refrigerant was expanded directly into the anodes at a steady state evaporation of −15 and −20 °C.

A planar cathode/tubular anode cell was developed later [24]. In this design (Fig. 2(b)), only about 50% of

the surface of the anodes was active, the remainder being shielded by an anode mounting plate, so that more effective cooling was achieved and higher current efficiencies resulted.

3.2. *Cooling the 2.7 dm³ cells*

The rate of heat dissipation (Q) in an electrochemical reactor is given by

$$Q/\mathrm{J\,s^{-1}} = -I\Delta H/zF + IU \qquad (15)$$

where H is the reaction enthalpy, I the cell current and U the cell voltage. For the overall ozone cell reaction (5), $\Delta H^\circ = 12.9\,\mathrm{kJ\,(mol\,O_3)^{-1}}$, so the first term on the right hand side, for the reversible process, corresponds to $-8.7\,\mathrm{J\,s^{-1}}$ (at 298 K) and the second term for the irreversible processes, to $192\,\mathrm{J\,s^{-1}}$ (for 4.8 V). The mean temperature of the electrolyte will be determined by Equation 15 less heat losses due to:

(i) heat transfer through the refrigerated anode by conduction;

(ii) heat transfer by conduction through the reactor walls;

(iii) heat in the evolved (low heat capacity) gases; and

(iv) latent heat to saturate the gases with water vapour.

The heat dissipated at the anode is of prime concern, because of the sensitivity of ozone current efficiency to temperature (Fig. 11). The reversible heat formation due to the overall anode reaction at 30% ozone current efficiency may be estimated [27] as $-0.452\,\mathrm{kJ\,m^{-2}\,s^{-1}}$, this is negligible ($\sim 4\%$) in comparison with the irreversible heat formation of $-11.6\,\mathrm{kJ\,m^{-2}\,s^{-1}}$, assuming an overpotential of about 2.9 V at $4\,\mathrm{kA\,m^{-2}}$. The heat generated at the anode/electrolyte interface operated at high overpotential/high current density is dissipated by: (i) bubble assisted convective heat transfer between the anode and bulk electrolyte; (ii) by conduction through the vitreous carbon anode driven by the temperature gradient resulting from;

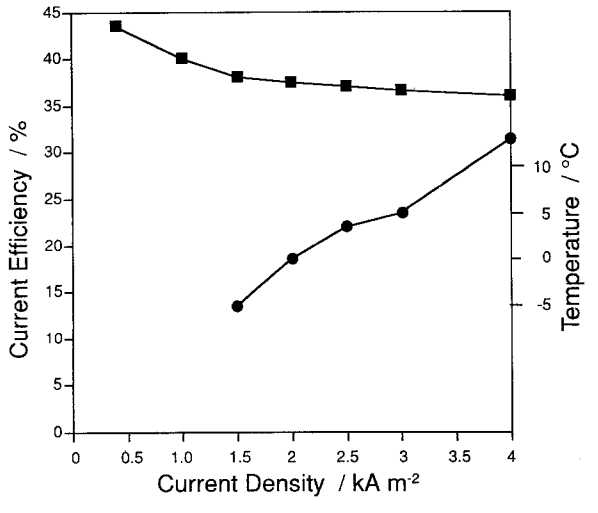

Fig. 11. Ozone current efficiency and temperature profile in 40 A, $0.010\,\mathrm{m^2}$ anode area, $2.5\,\mathrm{dm^3}$, cylindrical cells.

and (iii) forced convective boiling of the refrigerant inside the anode.

Heat transfer coefficients at gas evolving electrode surfaces are dependent on the gas evolution rate; correlations available in the literature [e.g. 28] could be used to model the heat transfer between the anode surface and the bulk electrolyte. However, the current density distribution/local gas generation rate would have to be solved simultaneously with the ohmic thermal dissipation and heat transfer between electrolyte and the anode as a function of height, though the very high apparent overpotentials would have a considerable smoothing effect on the more usual bubble-induced current density distortions [e.g. 29–31].

For the case of a homogeneous electrolyte in the annular interelectrode gap, the overall electrolyte resistance (R) is

$$R = \frac{\rho}{2\pi L}\int_{r_{a,o}}^{r_c}\frac{dx}{x} = \frac{\rho}{2\pi L}\ln\left(\frac{r_c}{r_{a,o}}\right) \qquad (16)$$

from which the local and total Joule energy dissipation can be calculated. For an HBF_4 specific conductivity of $50\,\Omega^{-1}\,\mathrm{m^{-1}}$ and a cell current of 40 A, this predicts an ohmic potential drop in a bubble-free electrolyte of 0. 33V for the specified geometric parameters, compared with the measured ohmic potential drop (~ 0.5 V), which includes the effect of gas bubbles [32–38].

Under steady state conditions, the rate of generation of bubbles is

$$Q_{O_3+O_2}/\mathrm{m^3\,s^{-1}} \simeq \frac{IV_M}{F}\left(\frac{\Phi_{app}}{6} + \frac{(1-\Phi_{app})}{4}\right) \qquad (17)$$

At the low temperature of electrolyte used, the effect of water vapour can be ignored. Hence, in principle, the mean increase in electrolyte resistance can be calculated from an appropriate correlation between the effective $(\rho_{eff})/(\rho_{bulk})$ bulk resistivity and the gas: electrolyte phase ratio (α_G/α_e) [e.g. 31–37]. However, this requires a knowledge of the mean bubble size [38] and hence their rise rate, and spatial distribution of their concentration in both radial and vertical directions [e.g. 35]; the resulting temperature distribution could then be computed numerically.

The greatest difficulties in providing cooling a $2.7\,\mathrm{dm^3}$ cell via the anode alone lie in achieving both sufficient heat transfer and sufficient refrigerant expansion inside the relatively small volume of the anode. The heat transfer rate (Q) through the annular anode of outer and inner radii $r_{a,o}$ and $r_{a,i}$, respectively, with a temperature differential of $T = T_0 - T_i$, is

$$Q = \frac{2\pi L k_T \Delta T}{\ln(r_{a,o}/r_{a,i})} \qquad (18)$$

where k_T is the thermal conductivity of the vitreous carbon anode of length L. Hence, for the heat transfer through the 0.003 m wall thickness of 0.0254 m o.d. glassy carbon tubes with $k_T = 8.0\,\mathrm{W^{-1}\,m^{-1}\,K^{-1}}$ for 2500 °C glassy carbon and for a likely T of

30 °C, $Q = 550$ W, indicating that such conditions provide more than adequate capability to cool the entire cell, as

$$Q(\text{generated}) = 0.97 \times 5\,\text{V} \times 40\,\text{A} = 194\,\text{W}$$

Measures were taken to ensure the expansion took place at low pressure via the use of oversized suction lines, and adding volume to the refrigeration circuit through the use of an accumulator downstream of the anode (which would nevertheless be required to prevent frost-back to the compressor at lower currents). Heat exchange between the suction line and capillary was used to cool liquid refrigerant before entering the anode so that its heat need not be removed within the confines of the anode itself.

The rate at which the refrigerant R12 had to be expanded per kilowatt of refrigerating effect was $0.00825\,\text{kg s}^{-1}\,\text{kW}^{-1}$. Using −15 and +25 °C as the bounds of the refrigeration cycle, the required compressor displacement was $5.87 \times 10^{-6}\,\text{m}^3\,\text{s}^{-1}\,\text{kW h}^{-1}$, and the theoretical power requirement was $208\,\text{W kW}^{-1}$, giving a theoretical coefficient of performance of 4.8.

Alternate refrigerants such as R502 and R22 have lower boiling points than R12, and as such allow the anode surface to achieve lower temperature. Compressors are designed for specific use with such refrigerants, due to their higher operating pressures, and are generally not available in a size appropriate for the 40 A cells. R502 and R22 would be preferable in larger-scale systems where yields and anode stability may consequently be improved.

The use of R502 in these experiments with R12 compressors was possible only with a water-cooled condenser; using air cooling, compressor overheating and consequent thermal cut-out took place. Figure 11 illustrates the ozone current efficiencies observed in a divided concentric cylinder $0.010\,\text{m}^2$ anode area cell with anodes internally cooled by the expansion of R502. The temperature rise in these $2.5\,\text{dm}^3$ cells contributed to a decline of current efficiency at higher current densities; without such cross-coupling parameters, ozone current efficiency rose to a plateau extending from approximately 3 to $6\,\text{kA m}^{-2}$.

Figure 12 shows the cell voltages observed in the $0.010\,\text{m}^2$ cells; again note the rise in steady-state temperature. Figure 13 shows the current efficiencies obtained as a function of temperature in planar cathode/tubular anode cells [24]. The improved cooling in these reactors enabled separation of variables.

3.3. *Option of using a separator*

It is clear from the literature [39] on ozone solubilities that few reliable data exist, with values for sulphuric acid being quoted variously as 0.03–$22\,\text{mol}\,O_3(aq)\,\text{m}^{-3}$ depending on temperature, ozone partial pressure and, to a far lesser extent, pH. Thermodynamic data from the most recent NBS listing [40] enables the following relationship to be

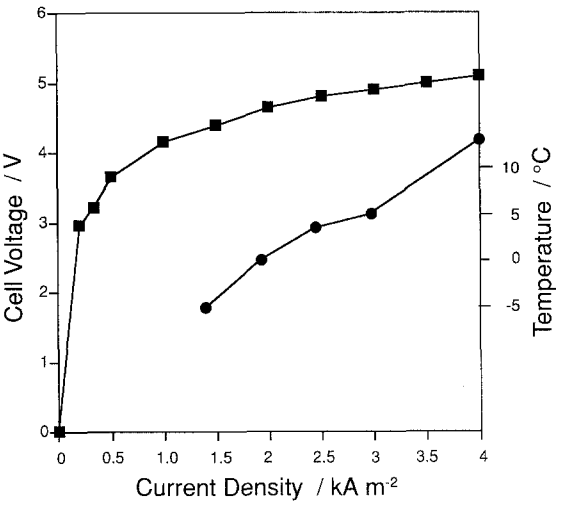

Fig. 12. Cell voltage and temperature profile in 40 A, $0.010\,\text{m}^2$. Anode area: $2.5\,\text{dm}^3$, cylindrical cells.

calculated, from which the ozone solubility at 298 K and 0.1 MPa O_3, can be calculated as $12.3\,\text{mol m}^{-3}$:

$$O_3(g) \Leftrightarrow O_3(aq) \qquad (19)$$

$$\log(O_3(aq)) = -1.91 + \log p\,O_3$$

which is an order of magnitude greater than that of oxygen ($1.23\,\text{mol}\,O_2\,\text{m}^{-3}$):

$$O_2(g) \Leftrightarrow O_2(aq) \qquad (20)$$

$$\log(O_2) = -2.86 + \log p\,O_2$$

The same Gibbs energy of formation of dissolved ozone also enables calculation of the reversible potential for its reduction by Reaction 21 at the air cathode:

$$O_3(aq) + 6H^+ + 6e^- \Leftrightarrow 3H_2O \qquad (21)$$

$$E/\text{V} = 1.53 - 0.0591\,\text{pH} + 0.0099\log(O_3(\text{aq}))$$

which would result in the apparent loss of anode current efficiency for ozone generation. As the air cathode operates at about +0.5 Vvs SHE, it is reasonable to assume that Reaction 21 would be mass transport controlled with a limiting current density (i_L) given by

$$i_L = 6F\frac{D_{O_3}}{\delta}c_{O_3} \qquad (22)$$

The ozone solubility under actual cell conditions was

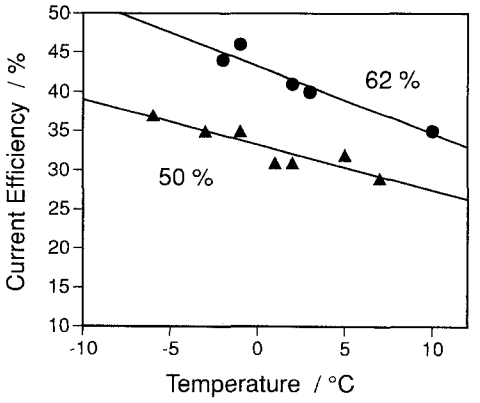

Fig. 13. Effect of temperature in planar/tubular cells using 50 wt % and 62 wt % HBF_4. Planar/tubular cell: $3.8\,\text{kA m}^{-2}$ [24].

determined by integrating the decay of ozone concentration vented from an electrolyte tank of known volume sparged with air subsequent to interrupting the current; a solubility of 60 mol m^{-3} was obtained at the bulk electrolyte temperature of 15–20 °C. That the experimental ozone concentration was greater than that predicted from Equation 19, may be ascribed to the temperature being lower than 298 K, inaccuracy of those data for such reactive species, that the activity of ozone in fluoboric acid is less than unity, or that the electrolyte was supersaturated in dissolved gas, as is often the case with such systems.

The bubble-induced enhancement in mass transport rates to surfaces such as the air cathode in close proximity to gas-evolving electrodes, the turbulent diffusion created enhances mass transport rates according to the correlation [41]:

$$Sh = 0.19(ScAr^*)^{1/3} \quad (23)$$

where Ar^* is a modified Archimedes number, defined, as in the case of the Sherwood number (Sh), with bubble diameter (d_b) as the characteristic length. If a gas phase fraction in the electrolyte voidage of 0.11 [42] and bubble diameter of 10^{-4} m is used to define $Ar^{1/3}(= 1.07)$ and a value of 1000 is chosen for the Schmidt number (Sc), then Equation 22 predicts a mean mass transport coefficient (k_m) of 1.5×10^{-5} m s^{-1}.

The time dependence of ozone concentrations at start up can be modelled approximately with the following assumptions:

(i) the undivided electrochemical reactor operates under quasi steady state conditions as a continuously stirred tank reactor of volume V;

(ii) the anode, of area A_a, is operated at a current density i_a, resulting in kinetically controlled ozone generation at a current efficiency, which is assumed to be independent of that current density at the first level of approximation. Data (e.g. Fig. 14) from experiments on reactors incorporating membranes/separators could be incorporated into the model to relax this assumption;

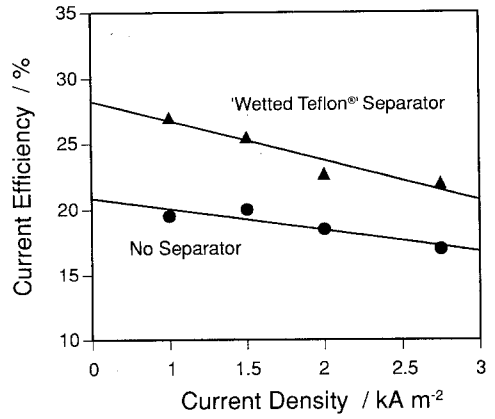

Fig. 14. Comparison of current efficiencies with and without a separator. Temperature: −5 to 0 °C. Fluoboric acid concentration: 60 wt %. Concentric cylinder cell.

(iii) transport controlled reduction of O_3 occurs at the cathode, of area A_c, operated at a total current density i_c, most of which is used for the reduction of atmospheric oxygen:

(iv) ozone gas desorption occurs at the electrolyte/gas interface of area A_L with a rate constant k_L. The surface ozone concentration ($[O_3]_s$) at the electrolyte/gas interface is in equilibrium with the gas phase ozone at partial pressure P_{O_3}, which is a measure of the apparent current efficiency (Φ_{app}), allowing for cathodic reduction losses in the undivided cell.

Then,

$$\frac{\Phi i_a A_a}{6F} - k_m A_c[O_3] - k_L A_L\{[O_3] - [O_3]_s\} = V\frac{d[O_3]}{dt} \quad (24)$$

where the third term corresponds to the rate of ozone gas desorption at the electrolyte/gas interface, prior to its reaching the solubility limit, above which bubbles could form and radically increase the magnitude of k_L.

$$[O_3]_s = K_{O_3}P_{O_3} \quad (25)$$

The total gas pressure (P_T) above the electrolyte is

$$P_T = P_{O_3} + P_{O_2} + P_{H_2O} \quad (26)$$

However, for the low electrolyte temperatures required for high ozone current efficiencies, the water vapour partial pressure could be neglected.

$$\Phi_{app} = \frac{P_{O_3}}{P_{O_3} + P_{O_2}} \quad (27)$$

$$\Phi_{app} = \Phi - \frac{6Fk_m A_c[O_3]}{i_a A_a} \quad (28)$$

$$\frac{\Phi i_a A_a}{6F} - [O_3]\{k_m A_c + k_L A_s\} + k_L A_L K_{O_3}(P_T - P_{H_2O}) \times \left\{\Phi - \frac{6Fk_m A_c[O_3]}{i_a A_a}\right\} = V\frac{d[O_3]}{dt} \quad (29)$$

$$\Phi\left[\frac{i_a A_a}{6F} + k_L A_L K_{O_3}(P_T - P_{H_2O})\right] - [O_3]\left\{k_m A_c + k_L A_s + \frac{6F_m A_c k_L A_L K_{O_3}(P_T - P_{H_2O})}{i_a A_a}\right\} = V\frac{d[O_3]}{dt} \quad (30)$$

Integration of Equation 30 by variable substitution, with the boundary condition $t = 0$, $[O_3] = 0$, results in the approximate expression for the time dependent

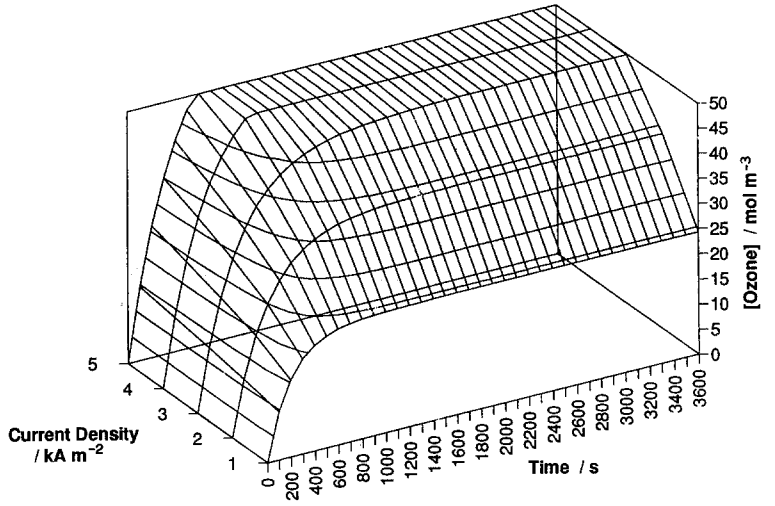

Fig. 15. Time dependence of ozone concentration, calculated from Equation 31, for the data: electrolyte volume, $V = 10^{-3}\,m^3$; anode area, $A_a = 0.01\,m^2$; cathode area $A_c = 0.02\,m^2$; cathode mass transport rate constant, $k_m = 1.5 \times 10^{-5}\,m\,s^{-1}$; ozone current efficiency, $= 0.6$, Faraday constant, $F = 96\,485\,As\,mol^{-1}$; ozone solubility, $[O_3]_{sat} = 50\,mol\,m^{-3}$, Ozone Henry constant, $K_{O_3} = 125\,mol\,m^{-3}$ (Equation 19), Total gas pressure, $P_T = 1$atm., electrolyte/gas interface area $A_L = 0.01\,m^2$, ozone gas desorption rate constant, $k_L = 1.5 \times 10^{-4}\,m\,s^{-1}$, $P_{H_2O} = 0.01$ atm.

ozone concentration:

$$[O_3]_t = \left[\frac{\Phi\left(\frac{i_a A_a}{6F} + k_L A_L K_{O_3}(P_T - P_{H_2O})\right)}{k_m A_c + k_L A_L + \frac{6F k_m A_c k_L A_L K_{O_3}(P_T - P_{H_2O})}{i_a A_a}}\right] \times \left\{1 - \exp\left[\frac{-t}{V}\left(k_m A_c + k_L A_s + \frac{6F k_m A_c k_L A_L K_{O_3}(P_T - P_{H_2O})}{i_a A_a}\right)\right]\right\} \quad (31)$$

which is plotted in Fig. 15, for the following data set:

Electrolyte volume, $V = 10^{-3}\,m^3$
Anode area, $A_a = 0.01\,m^2$
Cathode area, $A_c = 0.02\,m^2$
Cathode mass transport rate constant, $k_m = 1.5 \times 10^{-5}\,m\,s^{-1}$
Ozone current efficiency, $\Phi = 0.6$
Faraday constant, $F - 96\,485\,As\,mol^{-1}$
Ozone solubility, $[O_3]_{sat} = 50\,mol\,m^{-3}$
Ozone Henry constant, $K_{O_3} = 125\,mol\,m^{-3}$ (Equation 19)
Total gas pressure, $P_T = 1$ atm.
Electrolyte/gas interface area $A_L = 0.01\,m^2$
Ozone gas desorption rate constant, $k_L = 1.5 \times 10^{-4}\,m\,s^{-1}$
$P_{H_2O} = 0.01$ atm.

As expected for a kinetically controlled formation reaction coupled to a transport controlled loss reaction, Fig. 15 predicts that saturation of the electrolyte with ozone is achieved only at higher current densities, the required time decreasing with increasing current density.

Similar calculations can be done for dissolved oxygen; as its solubility is estimated to be an order of magnitude lower than that of ozone, oxygen bubbles will form prior to ozone achieving its saturation concentration, the bubbles greatly increasing the magnitude of k_L.

The time dependence of the apparent current efficiency (Φ_{app}) for ozone generation can be calculated from Equation 30 and the data in Fig. 15, which results in the data shown in Fig. 16. Unfortunately, comparison with the experimental data shown in Figs 5 and 6 indicates poor agreement with the model. This arises from the assumption of current efficiency being independent of current density and the experimental data having the effects of temperature (Figs 11 and 13) confounded with those of current density. None the less, the model indicates the benefits of operating at higher current densities for constant temperature and anode current efficiency; this is reinforced when the specific electrical energy (using cell voltage data from Fig. 12) and space-time yields are considered, as shown in Figs 17 and 18, respectively.

Such improvements could be obtained with either lowering the anode surface temperature and/or using a cation exchange membrane such as a Nafion® (du Pont, Wilmington, Delaware) to decrease any ozone reduction at the air cathode. However, these measures would increase the cell voltage; an optimum needs to be defined. Increasing the ozone current efficiency will decrease the concentration of gas between the electrodes and hence decrease the electrolyte resistance, so further decreasing the specific energy requirement.

Oxygen solubilities and diffusion coefficients for Nafion® membranes have been reported [43]; similar data is needed for ozone to enable current efficiency losses in the presence of a membrane to be estimated.

To test the use of a separator Zitex®, a porous PTFE filtration septum material (Norton, Worcester, MA), was etched with a sodium metal dispersion in an aryl ether in order to make it temporarily hydrophilic. The mean pore size chosen for this purpose was, from the manufacturer's

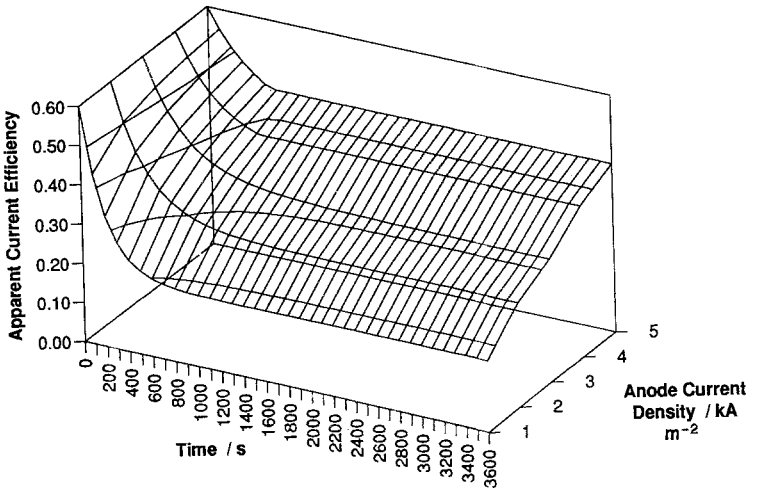

Fig. 16. Time dependence of the apparent current efficiency (Φ_{app}) for ozone generation calculated from Equations 28 and 31, for data in Fig. 15.

specifications, 3 to 6×10^{-5} m. A thickness of 1.78×10^{-4} m was used. Figure 14 shows current efficiency data obtained when using wetted Zitex® as a separator, indicating significant enhancement in apparent current efficiency due to decreased cathodic ozone reduction rates.

Wetted Teflon® produced by sodium metal dispersion etching techniques ultimately reverts to virgin Teflon®, as the surface is oxidized in the acid/ozone environment. Other materials containing specific graftings of stable ligands which wet the surface (i.e., sulphonic acid groups) may enable such a separator to have a useful operating lifetime.

Nafion® or other perfluorinated sulphonic acid membranes are used in the Membrel® cell and similar products, and thus, have proven stable to an ozone environment. Perfluorinated membranes should prove acceptable; however, in the reactors described here, water rebalance measures would be required to deal with accumulation in the catholyte due to electromigration and cathodic formation. Thus, a porous hydrophilic separator may be preferable if one can be identified that is compatible with the cell environment.

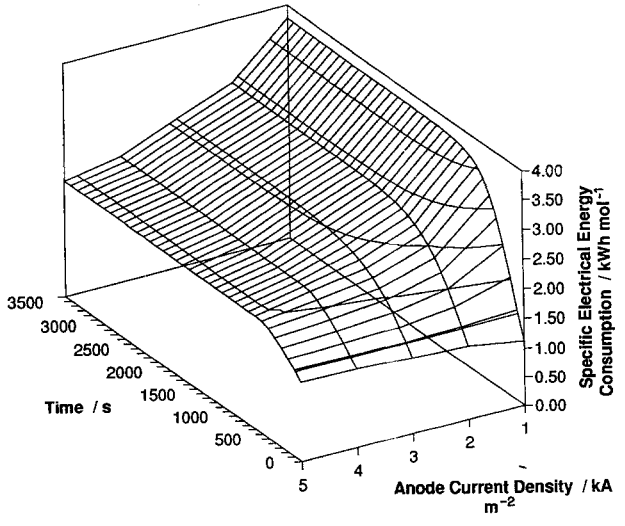

Fig. 17. Time dependence of specific electrical energy calculated from data in Fig. 15 and using cell voltage data from Fig. 12.

Other measures to decrease the concentration of dissolved ozone may be helpful; these include providing porous hydrophobic surface area in the electrolyte tank to promote bubble growth and so decrease ozone supersaturation. The introduction of diluent via sparging the electrolyte is also helpful.

3.4. *Process control*

The 40 A cylindrical cells (Fig. 1(a)) described above were incorporated into 0.067 m^3 stand-alone units, packaged into a standard 19 inch instrument casing. These were designed to be fully variable and were destined for research purposes. All utilities (air source, demisting, cooling, power supply, and process control) were on-board, giving a total weight of 35 kg.

The design of the small-scale apparatus presented several process control and safety-related problems that were best solved by incorporating a microprocessor. There was a need to ensure that hydrogen was never evolved. This could have occurred if the flow of feed air was accidentally shut off. This problem was approached by monitoring cell voltage on a continuous basis and comparing it to an internally stored current/voltage characteristic for the cell operating under normal conditions. Tolerance bands were set such that automatic shut-down occurred in the case that cell voltage rose above or fell below the specified range. (Protection against short circuits and cooling system failure also results from this approach.)

A second safety-related issue was encountered in limiting the ozone concentrations generated to (an arbitrarily determined) 15 wt %, a figure generally considered safe in the absence of organic or catalytic materials. Higher concentrations may be safe. For this, a flow of diluent is required at all times. A calorimetric flow switch was employed on the product line to provide a signal used by the microprocessor to

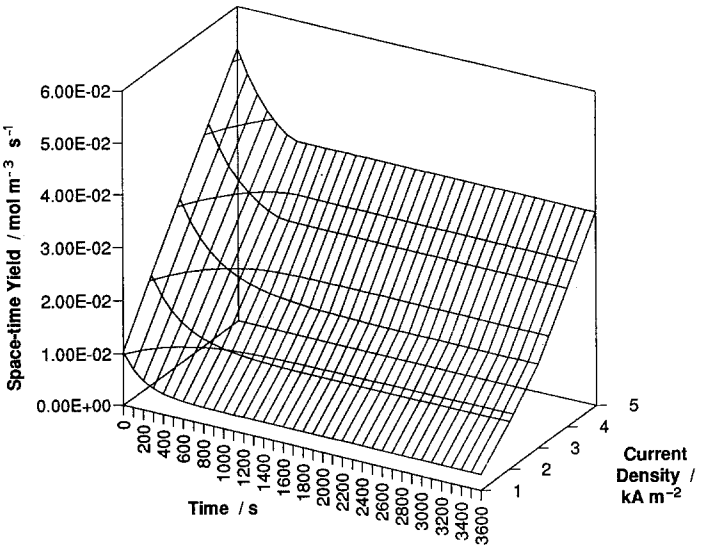

Fig. 18. Time dependence of space-time yields for data given in Fig. 15.

trip out the cell should the flow rate have fallen below a prescribed limit.

With the requirement of a microprocessor for satisfactory process control, it was then possible also to use it for additional (product related) features such as start-up and shut-down prompts. Further, it was possible to add internal translations between desired ozone generation rates and consequent amperage settings and feed air flow meter heights (as well as between the concentrations required and diluent flow meter heights). In effect, the current efficiency against current density curve and flow meter calibration curves were stored for use in translations and reminder messages. Diagnostic functions able to display current, cell voltage, and hours logged on the electrodes were added. Other logic functions included the use of a bimetallic switch to sense whether the cooling system was functioning, use of a venting period at shut-down, an on-delay on the monitoring system to allow time to reach steady-state operation, and the ability to have air flow in the absence of ozone generation for use in setting-up process flows. Electrolyte level was also monitored via the use of a float switch.

3.5. *Large scale reactor design*

The most promising large-scale reactor design option identified incorporated tubular glassy carbon anodes and planar cathodes, as shown schematically in Fig. 1(b) [24]. There is a limitation on the size of glassy carbon plates arising from losses in firing, concerns over breakage during cell assembly and sealing methods are a problem.

Submersed cells in a tank electrolyser may be preferable to a filter-press design. However, the alternative of using tubular anodes rather than planar anodes merits consideration, since simple O-ring seals can be used and there is a decreased susceptibility to fracture. Tubes are relatively inexpensive and are available commerically in a variety of diameters standard products up to a metre in length.

A tank electrolyser concept based on tubular anodes and planar cathodes is feasible. The design can incorporate shielding part of the anode surface in order to allow for the internal volume to surface area ratios required to achieve target surface temperature at high current density. Secondary cooling via the electrolyte is also possible.

A cathode coating may be necessary to restrict percolation of feed gas into the electrolyte, if there is a gradient by hydrostatic pressure over the cathode caused by exposing the cathode to too great a hydrostatic pressure, resulting from the immersion depth in the electrolyte.

4. Process economics

For small-scale equipment, purchasing decisions are apparently made on the basis of initial capital cost and ozone concentrations available rather than specific electrical energy consumption.

The following compares the components of cell voltage for the concentric cylinder cells:

40 A Cylindrical cell (48 wt % HBF_4)	
Anode potential at 4 kA m^{-2} (Vvs SHE)	4.1
Cathode potential at 2.25 kA m^{-2}(Vvs SHE)	0.4
Electrolyte IR estimate	0.5
($IR = (I/2L)\log(r_c/r_a) + 15\%$ for bubbles)	
Miscellaneous losses:	0.7
Current collection	
Cathode reinforcing internal to cell (if any)	
Adherent bubbles	
Total	**4.9 V**

From the cell voltage and current efficiency, the specific electrical energy consumption of the reactors themselves may be calculated:

Concentric cylinder reactor voltage:
4.9 V at $\Phi = 35\%$
Therefore, from Equation 6:
$SEEC = 46.9\,\text{kWh kg}^{-1}$
Heat generation to be removed:
97% of the above

To this, the specific energy consumption of refrigeration must be added in. This may be determined using the typical performance of refrigeration systems operating between a suction temperature of −15 °C and a discharge temperature of 35 °C (which would be a typical duty for R12). A factor of 0.35 results, which can then be applied to the heat generation of the cells to calculate the power consumption of refrigeration. Thus determined, 16.0 kWh kg^{-1} O_3 of refrigeration is required to cool the 40 A, 2.7 dm^3 cylindrical cells.

For the small-scale devices, a switched mode power source was used, as these have very high efficiencies. A 5 V source typically has an efficiency of 75%; the higher the voltage, the closer switched mode power supplies approach a limit of approximately 95% efficiency. For large-scale electrochemical systems direct rectification of mains is used, the efficiency of which is approximately 95%. Thus, 95% conversion efficiency may be assumed for all but the smallest devices.

If 4.5 V and 45% current efficiency are assumed, when added to power supply losses and refrigeration requirements, these characteristics would give a specific electrical energy consumption of approximately 33.5 kWh kg^{-1}, compared with 22 to 26 kWh kg^{-1} for air fed corona discharge systems generating 1 to 1.5 wt % ozone. In some applications, the advantages of high concentration ozone may off-set the inherent operating cost penalty of the electrochemical process.

Advantages in capital cost can be expected for an electrochemical process in that no feed air drying is required, and low-voltage, high-amperage d.c. power supplies are less expensive than high frequency, high-voltage a.c. power supplies. Further, the high current efficiencies observed at high current densities imply a specific generation rate per unit electrode area up to two to three times that of corona discharge.

5. Implications for applications engineering

Electrochemical approaches offer independent control of concentration and output. Full turn-down and programmability are also possible. Small-scale corona discharge technology does not offer these advantages. Further, electrochemical equipment is smaller, lighter, and less noisy. The specific advantages of higher ozone concentrations may be classified as follows.

Ozone oxidation of many organic chemicals proceeds as a multi-step process, though considering only the destruction of the parent compound, X, the reaction rate may be expressed [44];

$$-\mathrm{d[X]}/\mathrm{d}t = k_{\mathrm{obs}} C_{\mathrm{O_3}(aq)}[\mathrm{X}] \qquad (32)$$

where $k_{\mathrm{obs}} = nk$, the product of the actual rate constant, and the stoichiometric factor, n, reflecting oxidations of daughter products.

'Slow' ozone oxidation reactions, those with $k_{\mathrm{obs}} < 100\,\mathrm{mol^{-1}\,s^{-1}}$, depend on dissolved ozone concentration, and are generally not practically carried out with conventionally available air-fed corona ozone sources. When reaction rates, rather than mass transfer of gas-phase ozone into solution is the rate-limiting process, high concentration ozone can be especially beneficial in that its aqueous solubility is then increased.

The solubility of ozone in water follows Henry's law:

$$P = HC_{\mathrm{O_3}(aq)}$$

where P is the partial pressure of the gas above the liquid (kg m^{-3} air), and H is the Henry's law constant. At 20 °C, $H = 2.59$(kg gas) m^{-3} air per (kg gas) m^{-3} water [44]. (This corresponds to an ozone solubility of 16 mol m^{-3} at 0.1 MPa ozone partial pressure, i.e. the minimum pressure required for its generation as bubbles under ambient conditions, cf. 12.7 mol m^{-3}; calculated from Equation 19.)

The chemical kinetics of oxidations with ozone are often rapid and do not impose limitations on current commercial waste treatment processes, as mass transfer from the gas phase to the aqueous phase is rate determining. The ozone oxidations of phenol, chlorophenols, cresols, cyanide ion, sulphide ion, mercaptans, and many amines fall into this category, having observed rate constants of $\geq 10^4\,\mathrm{mol^{-1}\,s^{-1}}$.

High concentration electrochemical ozone can also be of benefit in these cases due to the improved mass transfer rates possible. An expression derived from film theory, where reaction rate is much faster than the diffusion of gas into liquid is [45]

$$\mathrm{N_{O_3}} = 2(\mathrm{C_{O_3 i}} - \mathrm{C_{O_3 l}})(D/t)^{1/2} \qquad (33)$$

From this expression, it is apparent that increasing ozone concentration will have a proportionate effect on increasing process throughput times, and may also decrease contactor volumes required, both of which decrease capital costs. For mass transfer controlled processes, electrochemically generated high concentration ozone may provide order of magnitude improvements.

If it is accepted that contactors costs increase with size to an exponent of 0.8, then a tenfold increase in ozone concentration can reduce contactor costs to approximately 1/6 present costs.

It is wholly dependent on the process being considered whether order of magnitude kinetic, solubility, or mass transfer advantages result in order of magnitude lower specific electrical energy consumptions (on a process as a whole basis), in decreased contactor vessel and gas handling equipment costs, in diminished plant footprint, or in decreased need for ozone generation capacity.

6. Future developments

Electrochemical ozone generators based on the principles discussed are being developed by Imperial Chemical Industries (Runcorn, Cheshire, UK) under licence from OxyTech, Inc. (Los Gatos, California,

USA). At present 40 A generators of $0.005\,kg\,h^{-1}$ fixed capacity are being produced for demonstration of the process technology, utility integration, and process control methods.

Trials of the technology for cooling tower water treatment are scheduled. This may be the most appropriate application, as relatively small-scale devices are required, high concentrations are important to achieve good solubility at elevated temperature, and the absence of air drying is important.

Acknowledgements

The participation of Electromedia Corporation (Englewood, New Jersey, USA) in producing and testing the air electrode material used in this study is gratefully acknowledged. Mr. Mark L. Goodwin of OxyTech is thanked for his many contributions to the program. Shaun Bullen, a chemical engineer with OxyTech (UK) Ltd and now of ICI Chemicals and Polymers, is thanked for his most vital hands-on contributions.

References

[1] S. Stucki and G. Theis, '*In situ* Production of Ozone in Water Using a SPE Electrolyse.' Paper 673, 163rd Meeting of the Electrochemical Society, 8–13 May (1983), San Francisco, CA.
[2] S. Stucki, G. Theis, R. Kotz, H. Davantay and J. J. Christen, *J. Electrochem. Soc.* **132**(2) (1985) 367–71.
[3] H. P. Klein and S. Stucki, 'The Production of Ozone by Electrolysis and its Application to High Purity Water Systems'. 7th Ozone World Congress, International Ozone Association, Tokyo, 9–12 September (1985).
[4] Chlorine Engineers Corporation Ltd., Shosen Mitsui Bldg., 1-1, Toranomon 2-chome, Minato-ku, Tokyo 105, Japan (Brochure, 1991).
[5] Permelec Electrode Ltd., 1159 Ishikawa, Fujisawa City, Kanagawa Prefecture, Japan (Brochure, 1991).
[6] M. Katoh, Y. Nishiki, and S. Nakamatsu, 'A Study on Electrochemical Ozone Generator Using Oxygen Gas Diffusion Cathode'. Meeting of the Japan Electrochem. Society, April 1992.
[7] E-TEK, Inc., 6 Mercer Road, Natick Industrial Park, Natick, MA 01760, USA.
[8] P. C. Foller and C. W. Tobias, *J. Electrochem. Soc.* **129** (1982) 505.
[9] P. C. Foller and M. L. Goodwin, *Ozone: Sci. & Engng* **6** (1984) 29–36.
[10] P. C. Foller and C. W. Tobias, 'Ozone Production by Electrolysis', *US Patent 4 316 782* (1982).
[11] P. C. Foller, M. L. Goodwin and C. W. Tobias, 'Electrodes for Ozone Production', *US Patent 4 375 395* (1983).
[12] P. C. Foller, 'Process and Device for the Generation of Ozone via the Anodic Oxidation of Water', *US Patent 4 541 989* (1985).
[13] C. A. Wamser, *J. Am. Chem. Soc.* **70** (1948) 1209–15.
[14] C. A. Wamser, *J. Am. Chem. Soc.* **73** (1951) 409–16.
[15] A. J. Bard, R. Parsons and J. Jordon (eds.), 'Standard Potentials in Aqueous Solution', Marcel Dekker, New York (1985).
[16] J. D. Seader and C. W. Tobias, *Ind. Eng. Chem.* **44**(9) (1952) 2207.
[17] T. R. Beck and R. W. Moulton, *J. Electrochem. Soc.* **103**(4) (1956) 247.
[18] D. P. Semchenko, E. T. Lyubushkina and V. Lyubushkin, *Electrokhimiya* **9**(11) (1973) 1744.
[19] P. C. Foller and C. W. Tobias, *J. Electrochem. Soc.* **129** (1982) 568.
[20] H. P. Fritz, J. C. G. Thanos and D. W. Wabner, *Z. Naturforsch.* **34B** (1979) 1617.
[21] J. C. G. Thanos, H. P. Fritz and D. W. Wabner, *J. Appl. Electrochem.* **14** (1984) 389.
[22] D. W. Wabner and J. C. G. Thanos, *J. Electroanal. Chem.* **182** (1985) 37.
[23] J. C. Hwang, 'Electrolytic Generation of Ozone'. Paper 592, 166th Meeting of the Electrochemical Society, New Orleans, 7–12 October (1984).
[24] A. M. Couper and S. Bullen, *in* 'Electrochemical Engineering and the Environment', I. Chem. E. Symp. Series No.127, I. Chem. E., Rugby (1992) pp. 49–58.
[25] N. Watanabe, T. Nakajima and H. Touhara, 'Graphite Fluorides', Elsevier, Amsterdam (1988) pp. 1–22.
[26] F. Solomon, *US Patent, 4 927 515* (1990).
[27] I. Rousar, K. Micka and A. Kimla, 'Electrochemical Engineering, Vol. 2, Elsevier, Amsterdam (1986).
[28] I. Rousar and V. Cezner, *Electrochim. Acta* **20** (1975) 289, 295.
[29] L. J. J. Janssen, G. J. Visser, *J. Appl. Electrochem.* **21** (1991) 753.
[30] J. M. Bisang, *ibid.* **21** (1991) 753.
[31] J. M. Bisang and G. Kreysa, *ibid.* **18** (1988) 422.
[32] R. E. Meredith and C. W. Tobias, *Adv. Electrochem. electrochem. Engng.* **2** (1965) 15.
[33] R. E. Meredith and C. W. Tobias, *J. Appl. Phys.* **31** (1960) 1270.
[34] H. Vogt, *J. Appl. Electrochem.* **17** (1987) 419.
[35] L. J. J. Janssen and G. J. Visser, *ibid.* **21** (1991) 386.
[36] L. Sigrist, O. Dossenbach and N. Ibl, *ibid.* **10** (1980) 223.
[37] H. Vogt, *in* 'Comprehensive Treatise on Electrochemistry', Vol. 6, (edited by E. Yeager, J. O' M. Bockris, B. E. Conway and S. Sarangapani), Plenum, New York (1983).
[38] H. Vogt, *Electrochim. Acta* **34** (1989) 1429.
[39] R. Battino (ed.), Solubility Data Series, Vol. 7, Pergamon/IUPAC, Oxford (1981).
[40] D. D. Wagman, W. H. Evans, V. B. Parker, R. H. Schumm, I. Halow, S. M. Bailey, K. L. Churney and R. L. Nuttall, *J. Phys. Chem. Ref. Data* **11** (Supplement 2) (1982).
[41] L. Sigrist, O. Dossenbach and N. Ibl, *Int. J. Heat Mass Transfer* **22** (1979) 1397.
[42] G. Kreysa and M. Kuhn, *J. Appl. Electrochem.* **15** (1985) 517.
[43] T. Sakai, H. Takenaka, E. Torikai, *J. Electrochem. Soc.* **133** (1986) 88.
[44] J. Hoigne, 'Mechanisms, Rates, and Selectivities of Oxidation of Organic Compounds Initiated by Ozonation of Water', in 'Handbook of Ozone Technology and Applications', (edited by R. G. Rice and A. Netzer) Ann Arbor Science, Ann Arbor, MI (1982) p. 341 *ff.*
[45] C.-H. Kuo and F. H. Yocum, 'Mass Transport of Ozone in Aqueous Systems', *ibid.* pp. 105 *ff.*